Journal of Physical Chemistry and Functional Materials

Home Page of Journal: https://dergipark.org.tr/jphcfum

The Effects of pH on the Morphology and Structural Properties of Er/Yb Co-Doped Hydroxyapatite

Bast Ahmed Mohammed[a], Tankut Ates [b, *], Bahroz Kareem Mahmood [c], Rebaz Obaid Kareem [c], Serhat Keser [d], Niyazi Bulut [e], Omer Kaygili [e]

[a] *Department of Applied Physics, College of Science, Charmo University, Chamchamal, Iraq*
[b] *Department of Engineering Basic Sciences, Faculty of Engineering and Natural Sciences, Malatya Turgut Özal University, Battalgazi, Malatya, Türkiye*
[c] *Physics Department, College of Science, University of Halabja, 46018, Halabja, Iraq*
[d] *Department of Chemical Technology, EOSB Higher Vocational School, Firat University, 23119, Elazig, Türkiye*
[e] *Department of Physics, Faculty of Science, Firat University, 23119 Elazig, Türkiye*
** Corresponding author: E-mail: tankut.ates@ozal.edu.tr*

ABSTRACT

The present study includes a detailed investigation of the effects of various pH conditions used in the synthesis on the structural properties of hydroxyapatite (HAp) co-doped with Er and Yb at a constant value. In this context, we changed the pH value from 8.5 to 11.0 with the steps of 0.5 in the synthesis. It was seen that the different pH causes significant variations in the crystallite size, lattice parameters, unit cell volume, and morphology. A biphasic structure composed of HAp and beta-tricalcium phosphate (β-TCP) was seen for all the samples, and the minor phase of the β-TCP phase almost disappeared for the samples having pH values of 10.5 and 11.0. The crystallite size (D), calculated using the Scherrer equation, varied between 28.1 nm and 36.8 nm. The pH value plays a key role in the synthesis of Er/Yb co-doped HAps.

ARTICLE INFO

Keywords:
Hydroxyapatite
pH
X-ray diffraction
FTIR

Received: 2024-03-21
Accepted: 2024-03-30
ISSN: 2651-3080
DOI:10.54565/jphcfum.1456331

1. INTRODUCTION

Hydroxyapatite (HAp) is a member of the calcium apatite family. Due to its chemical similarity to the mineral component of human bones (representing approximately 65-70% of bone mass) and dental hard tissues, it is widely researched as a bioceramic [1-3]. HAp, with the chemical formula $Ca_{10}(PO_4)_6(OH)_2$, is the most stable calcium phosphate salt at normal temperatures and pH values between 4 and 12 [4]. There are two phases known as hexagonal and monoclinic phases of HAp crystals [5]. The most commonly found structure of HAp is a stoichiometric apatite phase with a Ca/P ratio of 1.67, belonging to the hexagonal system with space group $P6_3/m$ [1, 4-6].

There has been a remarkable increase in publications related to HAp in recent years, especially concerning its biomedical applications [7]. Owing to its superior properties such as high biocompatibility, bioactivity, osteoconductivity, osteointegration, osteoinductivity, thermal and chemical stability, non-toxic and non-inflammatory nature, non-immunogenicity, porous structure, and low cost, HAp is a prominent biomaterial group for many fields [1, 4, 8-10]. Due to these advantageous properties, HAp is being researched and utilized in various fields such as orthopedics, maxillofacial surgery for implantation or prosthetics, repair or replacement of hard tissues, regeneration of diseased or damaged bones and teeth, scaffolds, bone fillers, controlled drug release, implant coatings, human body biomineralization, prevention of growth of many cancer cell types, dental enamel repair, desensitizing agents after tooth whitening, remineralization agents in toothpaste, treatment of early caries lesions, and many other areas [1, 2, 4, 5, 8, 9]. Besides biomedical applications, HAp is also used in various other fields such as chromatography, fertilizer, and pharmaceutical industries, catalysis, gas sensing, environmental remediation, water purification processes, fluorescent lamps, and fuel cell materials [1, 2, 6, 11, 12].

Despite offering excellent results in many areas, HAp has poor mechanical strength, low fracture toughness, brittleness, and low absorbability. The most suitable solution to overcome these disadvantages and further improve its properties is to modify the structure of HAp by doping with metal or non-metal ions. Various types of substitutions, especially anionic (PO_4^{3-}) and cationic (Ca^{2+}) substitutions, can address all the aforementioned drawbacks [10,13]. There are studies in

the literature regarding the doping of many elements such as Pr[14], Er[15], Dy[16], Y[17], Mg[18], Yb[19], Zn[20], Cd[21], Co[22], Ag[23], and Nb[24] into HAp. Pham et al. [25] demonstrated that effective near-infrared luminescence emission of HAp can be achieved through doping with the rare earth element erbium. Mondal et al. [26] confirmed the non-toxic properties of synthesized Er-doped HAp nanoparticles through *in vitro* bioactivity analysis. They also stated that these samples exhibited good luminescence properties, thus potentially serving as a promising material for biomedical imaging applications. Tang et al. [27] reported that Yb doping in bone scaffolds is a promising strategy to enhance osteogenic and angiogenic abilities for bone defect healing. Nardi et al. [28] determined that the Nd^{3+}-Yb^{3+} doped HAp nanoparticles could potentially be used not only as a diagnostic near-infrared down-shifting agent but also as a nanosystem for near-infrared photoactivated treatment.

Different methods are used to synthesize HAps, and each method causes the preparation of HAps to have different particle sizes, shapes, morphologies, densities, and crystallinities, depending on various synthesis conditions. Therefore, the physical, chemical, mechanical, and biological properties of HAp largely depend on the processing methods and conditions [29]. There are various synthesis methods for HAp, such as sol-gel [30], hydrothermal [31], ultrasonic, microwave [32], microemulsion [33], wet chemical synthesis [34], double decomposition method [35], and chemical precipitation [36].

Experimental factors such as stoichiometry, pH, calcination temperature, and reactive addition rate affect the precipitation of HAp, so it is crucial to control these factors for producing HAp with optimum morphology and crystallinity [6,11]. Lopez-Ortiz et al. [37] observed the effect of pH on the microstructure and morphology of HAp synthesized by the hydrothermal method. They reported an increase in monoclinic phase formation and a decrease in hexagonal phase formation as pH decreased, along with a decrease in crystallite size. They explained the role of pH in influencing the properties of HAp, indicating its correlation with the amount of H^+ and OH^- ions present in the solution. Sánchez-Campos et al. [38] demonstrated the effect of pH on the main physicochemical properties of HAp synthesized by microwave-assisted hydrothermal method, observing an increase in monoclinic phase from 85% to 95% with pH increase and a decrease in hexagonal phase from 15% to 5%, noting that the pH determined for synthesis adjusted the particle and crystallite sizes and shapes. Lee et al. [39] commented on the effect of pH, noting that as pH decreased, the concentration of H^+ ions in the reacting solution increased, leading to an increase in the concentration of HPO_4^{2-} due to combinations with PO_4^{3-} ions, resulting in Ca-deficient HAp formation. However, an opposite effect was observed as pH increased, leading to stoichiometric HAp formation. Rodríguez-Lugo et al. [40] found that carbonate stretching modes decreased with increasing pH and that the H–O–H antisymmetric stretching mode was eliminated for powders sintered at 900°C, confirming the formation of stable and porous HAp powders. Awan et al. [41] concluded that calcination has a significant effect on crystallite size, but conversely, the acidity and alkalinity (pH) of the solution have a more pronounced effect on particle size and morphology. Sun et al. [42] stated that morphology could be controlled by altering the pH of the reaction. Chuprunov et al. [43] investigated the effects of raising the pH level from 7 to 11 on the structure and found that while at pH 7, biphasic structures such as $CaPO_3(OH)$ and $Ca(OH)_2$ were detected, $Ca_{9.04}(PO_4)_6(OH)_{1.68}$ and $CaHPO_4$ were observed at pH 9, and single-phase HAp was obtained at pH 11.

In this study, Er and Yb co-doped hydroxyapatites were synthesized via the chemical precipitation method. Six different HAp samples synthesized at pH values of 8.5, 9.0, 9.5, 10.0, 10.5, and 11.0 will be examined to investigate the effect of pH on crystal structure and morphology.

2. MATERIAL AND METHOD

As the starting chemicals, calcium nitrate tetrahydrate, ytterbium (III) nitrate pentahydrate, erbium (III) nitrate pentahydrate, and diammonium hydrogen phosphate were purchased from Sigma-Aldrich and used without any further purification. 100 mL of the solution of 49.850 mmol calcium nitrate tetrahydrate, 0.075 mmol ytterbium (III) nitrate pentahydrate, and 0.075 mmol erbium (III) nitrate pentahydrate was prepared. 100 mL of 30.0 mmol of diammonium hydrogen phosphate solution was prepared, then poured drop by drop into the first solution. For preparing each sample, in this step, the pH was adjusted to 8.5, 9.0, 9.5, 10.0, 10.5, and 11.0 by adding an ammonia solution (Sigma-Aldrich). The final solution was stirred for 2 h without heating and then filtered two times using distilled water. The as-filtered samples were dried in an oven at 110 °C for 52 h. As a final step, the as-dried samples were calcined in an electrical furnace at 880 °C for 3 h, and the HAp powders were obtained.

The characterization of the crystal structure was conducted utilizing X-ray diffraction (XRD) technique employing the Bruker D8 Advance diffractometer. Fourier-transform infrared (FTIR) spectroscopy analyses were done using the Perkin Elmer Spectrum One spectrophotometer via the potassium bromide (KBr) method. Morphological observations were obtained using an FEI Quanta 450 FEG model scanning electron microscope.

3. RESULTS AND DISCUSSIONS

3.1. XRD analysis

The XRD results of HAp samples prepared at different pH values are shown in Fig. 1. The crystal structure-related peaks are pointed out in these patterns. Two phases are observed. The major one is the HAp (PDF No: 09–0432) and its Miller indices are shown in black. The minor phase is the β-TCP (PDF No: 09–0169) and the peaks having blue color with the ◆ symbols on the XRD patterns represent this minor phase. is observed. For this study, it is observed that the intensities of the peaks related to the β-TCP phase decrease continuously with increasing pH value. This phase almost disappears for the samples prepared at the pH values of 10.5 and 11.0. The formation of the single-phase of HAp at the pH of 11 was reported by Chuprunov et al. [43].

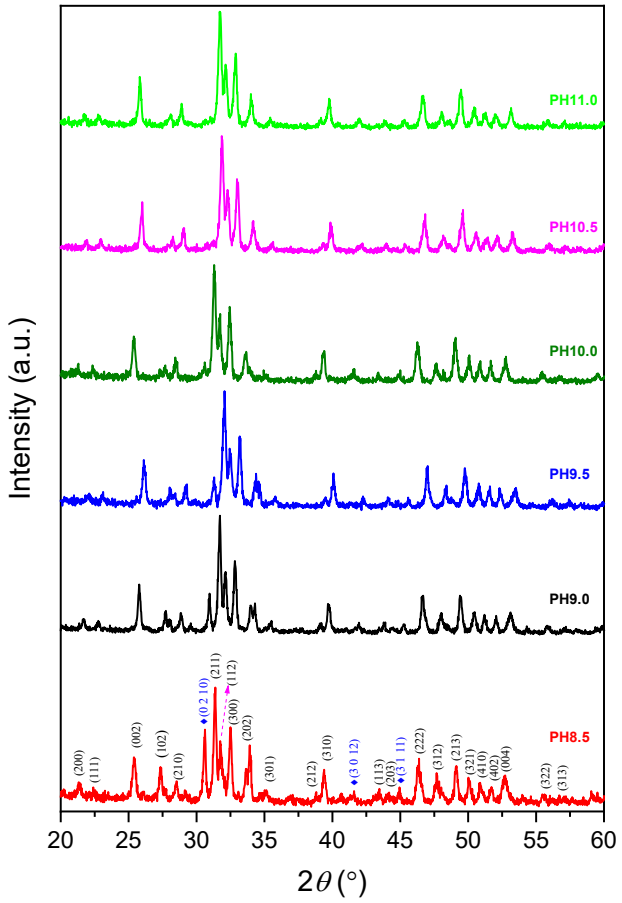

Fig. 1. XRD patterns of the samples

The crystallite size (D) was calculated by using the Scherrer equation [44],

$$D = \frac{0.9\lambda}{B_{1/2}\cos\theta} \quad (1)$$

where λ is the wavelength, $B_{1/2}$ is the full width at half maximum, and θ is the diffraction angle. The details of the calculation of the lattice parameters (a and c) and unit cell volume (V) can be found elsewhere [45].

Table 1. XRD analysis results

Sample	D (nm)	a (nm)	c (nm)	c/a	V (nm)^3
HAp*		0.9418	0.6884	0.7309	0.5288
PH8.5	34.6	0.9536	0.7008	0.7349	0.5519
PH9.0	36.8	0.9449	0.6906	0.7309	0.5340
PH9.5	29.1	0.9351	0.6817	0.7290	0.5162
PH10.0	28.1	0.9553	0.7013	0.7341	0.5542
PH10.5	34.2	0.9379	0.6849	0.7302	0.5218
PH11.0	32.5	0.9428	0.6890	0.7308	0.5304

* points out the standard data belonging to the JCPDS card with the number 09-0432.

3.2. FTIR analysis

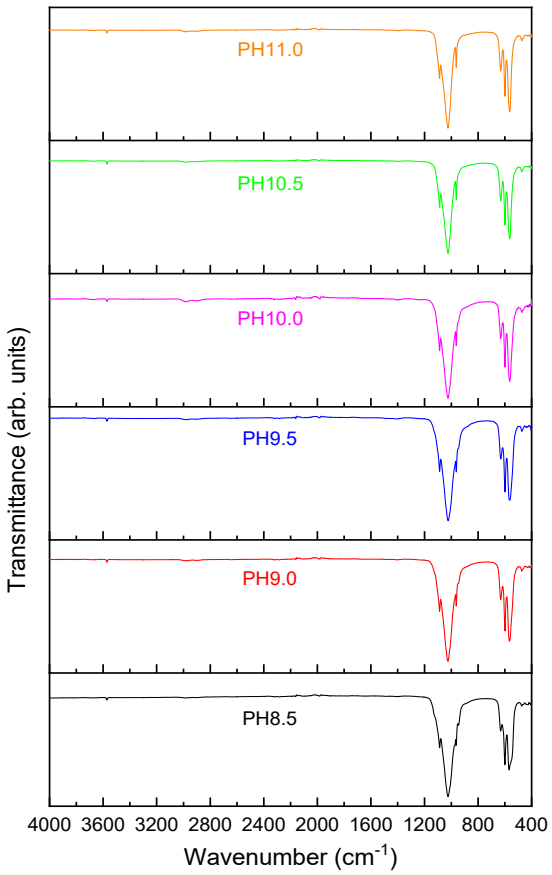

Fig. 2. FTIR spectra of the as-prepared HAp samples

Fig. 2 illustrates the FTIR spectrum for each sample in the wavenumber range from 400 to 4000 cm^{-1}. The as-detected bands and their assignments are given as follows. The bands observed at 1086 and 1024 cm^{-1} are associated with the anti-symmetric stretching mode of the P–O bond [46]. The bands 945 and 962 cm^{-1} are assigned to the symmetric stretching mode of the P–O bond [47]. The bands detected at 600 and 567 cm^{-1} are related to the bending mode of the O–P–O bond [48]. The 473 cm^{-1} band is assigned to the bending mode of the phosphate group [49]. The bands detected at 632 and 3574 cm^{-1} are related to the vibrational modes of the hydroxyl group [50]. Both groups observed in the FTIR spectra verify the formation of HAp structure [51].

3.3. SEM and EDX results

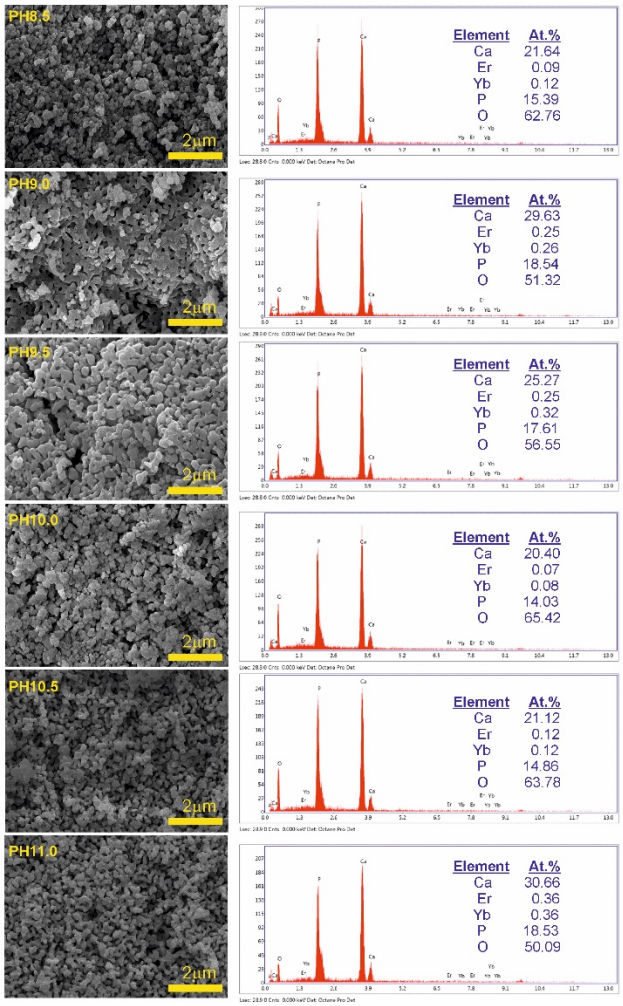

Fig. 3. SEM and EDX results

The SEM micrographs of the samples are shown in Fig. 3. It can be seen that the morphology, especially the particle sizes, is affected by the pH conditions used in the synthesis. All the samples consist of nano-sized particles. The EDX results confirm that each sample includes the elements of Ca, P, O, Er, and Yb. The amount of Er and Yb is found to be so close to each other. Using the EDX results, the molar ratios of the (Ca+Er+Yb)/P are estimated to be 1.42, 1.63, 1.47, 1.47, 1.44 and 1.69 for PH8.5, PH9.0, PH10.0, PH10.5, and PH11.0, respectively. The pH affects the (Ca+Er+Yb)/P and may be used for controlling the particle size distribution of the sample.

4. DISCUSSION

In the present work, six HAp samples with the same composition were prepared by using different pH conditions ranging from 8.5 to 11.0. The experimental analysis techniques of the XRD, FTIR, SEM, and EDX were used to determine the effects of the different pH values on the structural properties and morphology of the Er/Yb co-doped HAp structure. It was observed that the unit cell volume, lattice parameters, crystallite size, morphology, and particle size distributions of the samples were affected by the pH conditions. The pH can be used to control the structural properties and morphology of the Er and Yb co-doped HAps.

Competing interests

The authors declare that they have no competing interests.

References

[1] D. S. Gomes, A. M. C. Santos, G. A. Neves and R. R. Menezes. A brief review on hydroxyapatite production and use in biomedicine. Cerâmica. 2019;65:282-302. https://doi.org/10.1590/0366-69132019653742706.

[2] A. Haider, S. Haider, S. S. Han and I. K. Kang. Recent advances in the synthesis, functionalization and biomedical applications of hydroxyapatite: a review. Rsc Advances 2017;7(13):7442-7458. https://doi.org/10.1039/C6RA26124H.

[3] G. Molino, M. C. Palmieri, G. Montalbano, S. Fiorilli and C. Vitale-Brovarone. Biomimetic and mesoporous nano-hydroxyapatite for bone tissue application: A short review. Biomedical Materials. 2020;15(2):022001. https://doi.org/10.1088/1748-605X/ab5f1a.

[4] A. A. Majhooll, I., Zainol, C. N. A., Jaafar, A., Ha, M. Z., Hassan, M., Mudhafar, A. A. Majhool and A. Asaad. A brief review on biomedical applications of hydroxyapatite use as fillers in polymer. J. Chem. 2019;13:112-119. https://doi.org/10.17265/1934-7375/2019.03.004.

[5] X. Wang and Y. Han. Dependence of predicted bulk properties of hexagonal hydroxyapatite on exchange–correlation functional. Computational Materials Science. 2023;224:112153. https://doi.org/10.1016/j.commatsci.2023.112153.

[6] J. Kamieniak, P. J. Kelly, C. E. Banks and A. M. Doyle. Mechanical, pH and thermal stability of mesoporous hydroxyapatite. Journal of Inorganic and Organometallic Polymers and Materials. 2018;28:84-91. https://doi.org/10.1007/s10904-017-0652-3.

[7] M. S. F. Hussin, H. Z. Abdullah, M. I. Idris and M. A. A. Wahap. Extraction of natural hydroxyapatite for biomedical applications—A review. Heliyon. 2022;8(8):e10356. https://doi.org/10.1016/j.heliyon.2022.e10356.

[8] P. M. Sivakumar, A. A. Yetisgin, S. B. Sahin, E. Demir and S. Cetinel. Enhanced properties of nickel–silver codoped hydroxyapatite for bone tissue engineering: Synthesis, characterization, and biocompatibility evaluation. Environmental Research. 2023;238:117131. https://doi.org/10.1016/j.envres.2023.117131.

[9] M. A. Goldberg, M. R. Gafurov, O. N. Makshakova, S. V. Smirnov, A. S. Fomin, F. F. Murzakhanov and V. S. Komlev. Peculiarities of charge compensation in lithium-doped hydroxyapatite. Heliyon. 2024;10(4):e25291. https://doi.org/10.1016/j.heliyon.2024.e25291.

[10] V. Murugesan, M. Vaiyapuri and A. Murugeasan. Fabrication and characterization of strontium substituted chitosan modify hydroxyapatite for biomedical applications. Inorganic Chemistry Communications. 2022;142:109653. https://doi.org/10.1016/j.inoche.2022.109653.

[11] M. B. Mobarak, M. N. Uddin, F. Chowdhury, M. S. Hossain, M. Mahmud, S. Sarkar, N. I. Tanvir and S. Ahmed. Solid-state synthesis of poultry waste derived hydroxyapatite: Effect of calcination temperature on crystallographic parameters and biomedical competency. Journal of Molecular Structure. 2024;1301:137321. https://doi.org/10.1016/j.molstruc.2023.137321.

[12] A. Fihri, C. Len, R. S. Varma and A. Solhy. Hydroxyapatite: A review of syntheses, structure and applications in heterogeneous catalysis. Coordination Chemistry Reviews. 2017;347:48-76. http://dx.doi.org/10.1016/j.ccr.2017.06.009.

[13] D. E. Radulescu, O. R. Vasile, E. Andronescu and A. Ficai. Latest research of doped hydroxyapatite for bone tissue engineering. International Journal of Molecular Sciences. 2023;24(17):13157. https://doi.org/10.3390/ijms241713157.

[14] L. Ibrahimzade, O. Kaygili, S. Dundar, T. Ates, S. V. Dorozhkin, N. Bulut, S. Koytepe, F. Ercan, C. Gürses and A. H. Hssain. Theoretical and experimental characterization of Pr/Ce co-doped hydroxyapatites. Journal of Molecular Structure. 2021;1240:130557. https://doi.org/10.1016/j.molstruc.2021.130557.

[15] B. Demir, E. Karacaoglu and E. Ayas. Synthesis and characterization of luminescent Er^{3+}-doped natural fluorapatite. ECS Journal of Solid State Science and Technology, 2022;11(10):106001. https://doi.org/10.1016/j.ceramint.2020.03.152.

[16] F. İsen, O. Kaygili, N. Bulut, T. Ates, F. Osmanlıoğlu, S. Keser, B. Tatar, İ. Özcan, B. Ates, F. Ercan, I. Ercan and R. O. Kareem. Experimental and theoretical characterization of Dy-doped hydroxyapatites. Journal of the Australian Ceramic Society. 2023;59(4):849-864. https://doi.org/10.1007/s41779-023-00878-8.

[17] M. Megha, A. Joy, G. Unnikrishnan, M. Jayan, M. Haris, J. Thomas, E. Kolanthai and S. Muthuswamy. Structural and biological evaluation of novel vanadium/Yttrium co-doped hydroxyapatite for bone tissue engineering applications. Journal of Alloys and Compounds. 2023;967:171697. https://doi.org/10.1016/j.jallcom.2023.171697.

[18] L. Duta and V. Grumezescu. The Effect of Doping on the Electrical and Dielectric Properties of Hydroxyapatite for Medical Applications: From Powders to Thin Films. Materials. 2024;17:640. https://doi.org/10.3390/ma17030640.

[19] S. Acar, O. Kaygili, T. Ates, S. V. Dorozhkin, N. Bulut, B. Ates, S. Koytepe, F. Ercan, H. Kebiroglu and A. H. Hssain. Experimental characterization and theoretical investigation of Ce/Yb co-doped hydroxyapatites. Materials Chemistry and Physics. 2022;276:125444. https://doi.org/10.1016/j.matchemphys.2021.125444.

[20] Y. Wang and T. Wang. An amorphous Zn-doped hydroxyapatite with high ultraviolet reflectivity. Materials Letters. 2024;362:136036. https://doi.org/10.1016/j.matlet.2024.136036.

[21] M. S. Hossain, S. Tarannum, M. Kawsar, N. M. Bahadur and S. Ahmed. Synthesis of pure and Cd-doped hydroxyapatite for the photo-catalytic degradation of Amoxicillin and Ciprofloxacin: Crystallographic characterization using XRD. Journal of Hazardous Materials Advances. 2024;13:100406. https://doi.org/10.1016/j.hazadv.2024.100406.

[22] L. Yan, X. Wei, Z. Zhang, C. Wang, Y. Jia, L. Wang, Y. Yan and X. Fan. Cobalt-doped hydroxyapatite for bone tissue engineering: Synthesis, characterization and in vitro biocompatibility of real-time extract. Materials Today Communications. 2024;38:108554. https://doi.org/10.1016/j.mtcomm.2024.108554.

[23] G. Bansal, R. K. Gautam, J. P. Misra and A. Mishra. Synthesis and Characterization of Poly (Methyl Methacrylate)/Silver-Doped Hydroxyapatite Dip Coating on Ti6Al4V. Colloids and Surfaces A: Physicochemical and Engineering Aspects. 2024;689:133662. https://doi.org/10.1016/j.colsurfa.2024.133662.

[24] W. Korzeniewski and A. Witkowska. Dissolution of Nb-doped hydroxyapatite prepared via low-temperature mechanochemical method: Spectroscopy studies. Nuclear Instruments and Methods in Physics Research Section B: Beam Interactions with Materials and Atoms. 2023;545:165149. https://doi.org/10.1016/j.nimb.2023.165149.

[25] V. H. Pham, H. N. Van, P. D. Tam and H. N. T. Ha. A novel 1540 nm light emission from erbium doped hydroxyapatite/β-tricalcium phosphate through co-precipitation method. Materials Letters. 2016;167:145-147. http://dx.doi.org/10.1016/j.matlet.2016.01.002.

[26] S. Mondal, V. T. Nguyen, S. Park, J. Choi, L. H. Tran, M. Yi, J. H. Shin, C.-Y. Lee and J. Oh. Bioactive, luminescent erbium-doped hydroxyapatite nanocrystals for biomedical applications. Ceramics International. 2020;46(10):16020-16031. https://doi.org/10.1016/j.ceramint.2020.03.152.

[27] Y. Q. Tang, Q. Y. Wang, Q. F. Ke, C. Q. Zhang, J. J. Guan and Y. P. Guo. Mineralization of ytterbium-doped hydroxyapatite nanorod arrays in magnetic chitosan scaffolds improves osteogenic and angiogenic abilities for bone defect healing. Chemical Engineering Journal. 2020;387:124166. https://doi.org/10.1016/j.cej.2020.124166.

[28] M. V. Nardi, M. Timpel, E. Biondani, R. Ceccato, A. Chiappini and S. Dirè. Synthesis and characterization of Nd3+-Yb3+ doped hydroxyapatite nanoparticles. Optical Materials: X. 2021;12:100118. https://doi.org/10.1016/j.omx.2021.100118.

[29] R. K. Chadha, K. L. Singh, C. Sharma, A. P. Singh and V. Naithani. Structural and bioactive investigation of Sr and Sr-Zr doped hydroxyapatite: A comparative study. Materials Chemistry and Physics. 2024;314:128829. https://doi.org/10.1016/j.matchemphys.2023.128829.

[30] K. Janakiraman and S. Swamiappan. Synthesis of hydroxyapatite via sol–gel combustion route: A comparative analysis of single and mixed fuels. Materials Letters. 2024;357:135731. https://doi.org/10.1016/j.matlet.2023.135731.

[31] A. Prihanto, S. Muryanto, R. Ismail, J. Jamari and A. P. Bayuseno. Batch hydrothermal synthesis of nanocrystalline, thermostable hydroxyapatite at various pH and temperature levels. Inorganic Chemistry Communications. 2023;157:111301. https://doi.org/10.1016/j.inoche.2023.111301.

[32] J. Indira and K. S. Malathi. Comparison of template mediated ultrasonic and microwave irradiation method on the synthesis of hydroxyapatite nanoparticles for biomedical applications. Materials Today: Proceedings. 2022;51:1765-1769. https://doi.org/10.1016/j.matpr.2021.03.028.

[33] V. C. A. Prakash, I. Venda and V. Thamizharasi. Synthesis and characterization of surfactant assisted hydroxyapatite powder using microemulsion method. Materials Today: Proceedings. 2022;51:1788-1792. https://doi.org/10.1016/j.matpr.2021.05.059.

[34] E. S. Krishna and G. Suresh. Development and characterization of acicular nano-hydroxyapatite powder from wet chemical synthesis method. Materials Today: Proceedings. 2022;56:781-784. https://doi.org/10.1016/j.matpr.2022.02.256.

[35] H. Agougui, N. Sebeia, M. Jabli and Y. El-Ghoul. Synthesis of hydroxyapatite-sodium metasilicate via double decomposition method: Characterization and application to the removal of methylene blue. Inorganic Chemistry Communications. 2021;133:108986. https://doi.org/10.1016/j.inoche.2021.108986.

[36] N. M. Pu'ad, J. Alipal, H. Z. Abdullah, M. I. Idris and T. C. Lee. Synthesis of eggshell derived hydroxyapatite via chemical precipitation and calcination method. Materials Today: Proceedings. 2021;42:172-177. https://doi.org/10.1016/j.matpr.2020.11.276.

[37] S. López-Ortiz, D. Mendoza-Anaya, D. Sánchez-Campos, M. E. Fernandez-García, E. Salinas-Rodríguez, M. I. Reyes-Valderrama and V. Rodríguez-Lugo. The pH effect on the growth of hexagonal and monoclinic hydroxyapatite synthesized by the hydrothermal method. Journal of Nanomaterials. 2020;2020:5912592. https://doi.org/10.1155/2020/5912592.

[38] D. Sánchez-Campos, M. I. Reyes Valderrama, S. López-Ortíz, D. Salado-Leza, M. E. Fernández-García, D. Mendoza-Anaya, E. Salinas-Rodríguez and V. Rodríguez-Lugo. Modulated monoclinic hydroxyapatite: The effect of pH in the microwave assisted method. Minerals. 2021;11(3):314. https://doi.org/10.3390/min11030314.

[39] I. H. Lee, J. A. Lee, J. H. Lee, Y. W. Heo and J. J. Kim. Effects of pH and reaction temperature on hydroxyapatite powders synthesized by precipitation. Journal of the Korean

Ceramic Society. 2020;57:56-64. https://doi.org/10.1007/s43207-019-00004-0.

[40] V. Rodríguez-Lugo, T. V. K. Karthik, D. Mendoza-Anaya, E. Rubio-Rosas, L. S. Villaseñor Cerón, M. I. Reyes-Valderrama and E. Salinas-Rodríguez. Wet chemical synthesis of nanocrystalline hydroxyapatite flakes: effect of pH and sintering temperature on structural and morphological properties. Royal Society open science. 2018;5(8):180962. http://dx.doi.org/10.1098/rsos.180962.

[41] A. A. Awan, U. Liaqat and Z. Hussain. The effect of pH on the morphological transformation of nanocrystalline hydroxyapatite during wet chemical synthesis. Journal of the Korean Ceramic Society. 2023;60(6):1010-1027. https://doi.org/10.1007/s43207-023-00324-2.

[42] R. Sun, K. Chen, Z. Liao and N. Meng. Controlled synthesis and thermal stability of hydroxyapatite hierarchical microstructures. Materials Research Bulletin. 2013;48(3):1143-1147. http://dx.doi.org/10.1016/j.materresbull.2012.12.013.

[43] K. Chuprunov, A. Yudin, D. Lysov, E. Kolesnikov, D. Kuznetsov, D. Leybo, I. Ilinykh and A. Godymchuk. The pH level influence on hydroxyapatite phase composition synthesized with hydrothermal method. In IOP Conference Series: Materials Science and Engineering. 2020;731:012023. https://doi.org/10.1088/1757-899X/731/1/012023.

[44] B. D. Cullity. Elements of X-ray Diffraction, Addison, Wesley Mass: 1978. p. 127–131.

[45] H. G. Ateş, O. Kaygili, N. Bulut, F. Osmanlıoğlu, S. Keser, B. Tatar, B. K. Mahmood, T. Ates, F. Ercan, I. Ercan, B. Ates and İ. Özcan. Investigation of the structural, thermal, magnetic and cell viability properties of Ce/Sr co-doped hydroxyapatites. Journal of Molecular Structure. 2023;1283:135318. https://doi.org/10.1016/j.molstruc.2023.135318.

[46] N. Charczuk, N. Nowak and R. J. Wiglusz. Synthesis and investigation of physicochemical properties and biocompatibility of phosphate–vanadate hydroxyapatite Co-doped with Tb3+ and Sr2+ ions. Nanomaterials. 2023;13(3):457. https://doi.org/10.3390/nano13030457.

[47] M. E. Zarif, S. A. Yehia-Alexe, B. Bita, I. Negut, C. Locovei and A. Groza. Calcium phosphates–chitosan composite layers obtained by combining radio-frequency magnetron sputtering and matrix-assisted pulsed laser evaporation techniques. Polymers. 2022;14(23):5241. https://doi.org/10.3390/polym14235241.

[48] R. L. Frost, Y. Xi, R. Scholz, F. M. Belotti and A. Lopez. Infrared and Raman spectroscopic characterization of the phosphate mineral fairfieldite–Ca2 (Mn2+, Fe2+) 2 (PO4) 2· 2 (H2O). Spectrochimica Acta Part A: Molecular and Biomolecular Spectroscopy. 2013;106:216-223. https://doi.org/10.1016/j.saa.2013.01.008.

[49] M. S. Hossain and S. Ahmed. FTIR spectrum analysis to predict the crystalline and amorphous phases of hydroxyapatite: A comparison of vibrational motion to reflection. RSC advances. 2023;13(21):14625-14630. https://doi.org/10.1039/D3RA02580B.

[50] O. M. Gomez-Vazquez, L. R. Bernal-Alvarez, J. I. Velasquez-Miranda and M. E. Rodriguez-Garcia. Effects of Temperature on the Physicochemical Properties of Bioinspired, Synthetic, and Biogenic Hydroxyapatites Calcinated under the Same Thermal Conditions. Nanomaterials. 2023;13(17):2385. https://doi.org/10.3390/nano13172385.

[51] I. Uysal, F. Severcan and Z. Evis. Characterization by Fourier transform infrared spectroscopy of hydroxyapatite co-doped with zinc and fluoride. Ceramics International. 2013;39(7):7727-7733. https://doi.org/10.1016/j.ceramint.2013.03.029.